Applied Mathematical Modelling 98 (2021) 59–70

Contents lists available at ScienceDirect

Applied Mathematical Modelling

journal homepage: www.elsevier.com/locate/apm

Reduced 2D/1D mathematical models for analyzing inductive effects in submerged arc furnaces

Mads Fromreide[a,b,*], Dolores Gómez[b,c], Svenn Anton Halvorsen[a], Egil Vålandsmyr Herland[d], Pilar Salgado[b,c]

[a] NORCE Norwegian Research Centre AS, Universitetsveien 19, Kristiansand 4630, Norway
[b] Department of Applied Mathematics, University of Santiago de Compostela, Campus Vida, Santiago de Compostela, E-15782, Spain
[c] Technological Institute for Industrial Mathematics (ITMATI), Campus Vida, Santiago de Compostela, E-15782, Spain
[d] Elkem ASA Technology, Fiskåveien 100, Kristiansand 4621, Norway

ARTICLE INFO

Article history:
Received 24 February 2021
Revised 21 April 2021
Accepted 29 April 2021
Available online 15 May 2021

Keywords:
Metallurgy
Submerged arc furnaces
Induction
Proximity effects
Analytical 1D models
Dimensional Aanalysis

ABSTRACT

Mathematical models have been developed to investigate the quantitative behaviour of the current and power distributions in large submerged arc furnaces, usually fed by a low-frequency alternating source. Reduced 2D and 1D models will be used to investigate the electrical behaviour inside the furnace; in particular, these models will allow us to explain the inductive effects between the different regions and to compare the use of genuine AC models vs. DC approximations. The merits and limitations of the reduced models will be analyzed in terms of geometrical and physical parameters. The models are based on three-phase submerged arc furnaces for ferromanganese production, which are characterized by coke enriched regions (coke beds) under the electrodes. Mathematical analysis and computer simulations show how AC differs from the simpler direct current (DC). If the electrode-electrode distance is large, the current will mainly run horizontally between the electrodes. The unidimensional AC model shows that the distribution in the coke bed is largely influenced by the (parallel) currents in the metal. On the other hand, the corresponding DC model will predict constant current and power distributions here. Two-dimensional simulations reveal that this AC property will be preserved qualitatively also for realistic electrode-electrode distances. Hence, if there is a significant power contribution from horizontal currents in the coke bed (or slag), DC models should be avoided.

1. Introduction

Design and operation of metallurgical processes have been gradually improved through industrial experience, research, modern process control, new and/or improved measurements, etc. Nevertheless, due to high temperatures and several complexities, the design and operation of the processes are still to a large degree empirically based, and several process variations are not properly understood. An important knowledge gap is a fundamental understanding of three-phase alternating

* Corresponding author at: NORCE Norwegian Research Centre AS, Universitetsveien 19, Kristiansand 4630, Norway.
E-mail address: mafr@norceresearch.no (M. Fromreide).

https://doi.org/10.1016/j.apm.2021.04.034

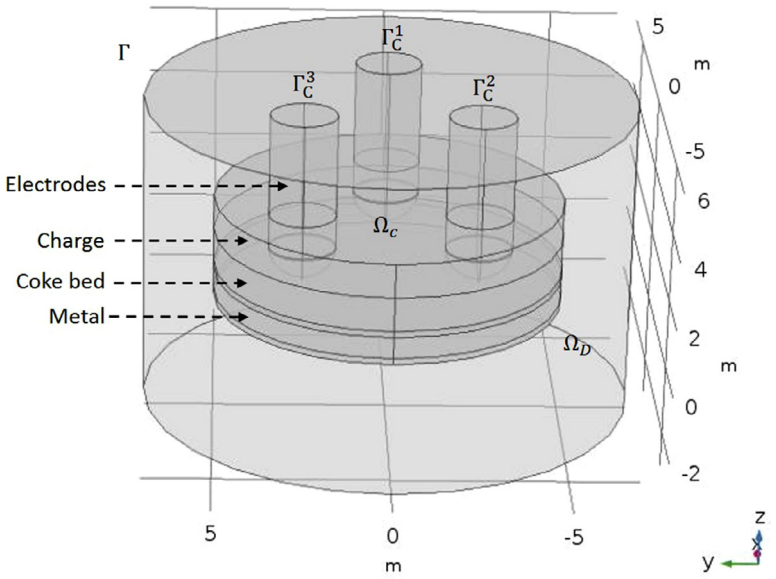

Fig. 1. Sketch of the 3D geometry.

currents (AC) [1]. An accurate understanding of the phenomena is important to calculate the power distribution, which affects the temperature distribution and also the chemical reactions inside the furnace.

Full 3D simulations of three-phase AC furnaces are complex and computationally costly. Therefore, many studies have focused on applying direct current (DC) models which reduce the complexity for faster approximations [1–8]. This cheaper DC approach is particularly relevant for multiphysics models [4–7]. However, inductive effects, such as the skin effect and proximity effects are not accounted for in this case. On the other hand, it is common to solve the full AC problem in the frequency domain, and calculate the electromagnetic power averaged over a period [9–12]. The AC approximation offers a realistic approximation, but it requires more computational effort if all the materials are included in the furnace; actually, the literature concerning AC 3D models in the whole furnace is quite few [10,13].

An important issue is whether the simplified DC models provide accurate estimates for real industrial furnaces. In the earlier "DC publications" this question has not been addressed. Based on the analysis of a non-dimensionalized equation, it can be shown that DC estimates will improve as the furnace size decreases [1], but this simple analysis does not supply quantitative guidelines for when the approximation can be appropriate or whether it should be avoided. Recently, Tesfahunegn et al. [13] performed a comparative analysis between AC and DC solvers for ferrosilicon furnaces by considering 3D simulations and different components in the furnace; however, this kind of comparison requires building 3D geometries for each specific case. In this paper, we will take advantage of reduced models for analyzing the sensitivity of the DC approximation without the need of expensive and specific computations.

We will investigate basic AC behaviour in submerged arc furnaces for typical material combinations within an industrial furnace, i.e., very good conductors (metals, electrodes) together with moderate conductors (slag, coke bed) and very low conducting and insulating materials (charge, insulating lining). We introduce first a fully 3D model as a basis for obtaining later a reduced 2D model. The 2D model is considered by both non-dimensional analysis and by numerical simulations. We also introduce an analytical 1D approximation of the 2D model for long and thin conductors, which is validated with numerical simulations with respect to different parameters. On the other hand, the 2D AC model is compared with DC simulations with varying electrode positions.

The studies are intended to get insight in some basic properties for large, three-phase AC furnaces to produce ferromanganese (FeMn). The results will, however, also be valid for similar furnaces, such as silicomanganese and ferrochrome furnaces, which also are characterized by a coke bed around the electrode tip.

2. Physical problem and mathematical model

Let us consider a three-phase AC submerged-arc furnace for production of FeMn [14]. The furnace consists of a cylindrical steel shell with three electrodes submerged in the charge material. A low frequency, normally 50 Hz, alternating current is supplied through the electrodes with $\pm 120^\circ$ shifts in the phase angles. The raw materials are heated through resistive heating and the charge is converted to metal and slag. An important characteristic is that carbon-enriched regions appear around the electrode tips. These regions are known as coke beds and have much higher electrical conductivity than the mixture layer above (see Fig. 1). This mixture layer (here referred to as charge layer) remains low conducting even at higher temperatures [14]. The current will mainly flow from the electrodes through the coke beds to the metal layer below. There-

fore the geometry of the coke beds plays an important role in the current distribution in the center of the furnace. The coke beds consist of a mixture of solid coke, and some liquid slag and liquid metal. The shape and conductivity distribution in the coke beds are difficult to measure and varies during the operation of the process [14–16]. In this work we consider the coke beds as uniform material, where the conductivity (for our reference case) is based upon reasonable bulk estimates given by Eidem [15].

For the mathematical model, we consider a simplified geometry where we will neglect the steel shell and furnace lining, and let the other material layers be approximated by cylindrical regions. Thus, we will distinguish a first layer placed at the bottom corresponding to the metal, a second one for the coke bed and a charge layer at the top. The electrodes consist of a highly conducting uniform material, and are submerged into the charge and coke bed layers, cf. Fig. 1.

2.1. 3D model

For introducing the reduced 2D/1D models, we first detail the components of a bounded 3D domain and the corresponding boundary conditions. The behaviour of electromagnetic fields are governed by Maxwell's equations. Since the electrodes are supplied with alternating current and the materials are assumed to be magnetically linear, the time harmonic approach is used. Moreover, as the operating frequency is low (50 Hz), the displacement term in the Ampere's law can be neglected (see, for instance, Bossavit [17]). Under these assumptions, the Maxwell system reduces to the well-know time-harmonic eddy current model, which reads

$$i\omega\mathbf{B} + \mathbf{curl}\ \mathbf{E} = \mathbf{0}, \tag{2.1}$$

$$\mathbf{curl}\ \mathbf{H} = \mathbf{J}, \tag{2.2}$$

$$\mathrm{div}\ \mathbf{B} = 0, \tag{2.3}$$

$$\mathbf{B} = \mu\mathbf{H}, \tag{2.4}$$

$$\mathbf{J} = \sigma\mathbf{E}, \tag{2.5}$$

where $\mathbf{H}$, $\mathbf{B}$, $\mathbf{E}$ and $\mathbf{J}$ are the complex amplitudes associated with the magnetic field, magnetic induction, electric field and current density, respectively; moreover, ω is the the angular frequency, $\omega = 2\pi f$, f being the frequency of the alternating current. The variable μ is the magnetic permeability of the material and σ its electrical conductivity, which is positive in conductors and zero in dielectrics. We will ignore temperature dependence of the properties and assume isotropic materials, hence μ and σ are constant within each material. Moreover, we have assumed that the magnetic permeability is equal to 1 for all materials.

These equations hold in the whole space. In order to solve them by using a finite element method we will restrict them to a cylindrical bounded domain Ω, containing the layers described above and the air around. We choose a Cartesian coordinate system (xyz) where the xy-planes are the horizontal planes of the furnace, and the z-axis indicates the vertical direction. We denote the orthonormal vector basis associated with the coordinate system by $\mathbf{e}_x$, $\mathbf{e}_y$ and $\mathbf{e}_z$. The domain Ω splits in two parts Ω_C and Ω_D, which consists of conductors (electrodes and furnace layers) and dielectric (air), respectively. Further we denote the boundary of Ω by Γ. The outer boundary of the conducting region, $\Gamma_C = \partial\Omega_C \cap \Gamma$, has three disjoint connected components Γ_C^n $(n = 1, 2, 3)$, representing the top of the electrodes. A sketch of the 3D geometry is shown in Fig. 1.

The model given by Eqs. (2.1)–(2.5) is completed with suitable boundary conditions, which will be chosen in order to impose voltage drops and/or currents on the top of the electrodes; namely, we will consider

$$\mathbf{E} \times \mathbf{n} = \mathbf{0} \qquad \text{on } \Gamma_C^n, \quad \text{for } n = 1, 2, 3, \tag{2.6}$$

$$\mu\mathbf{H} \cdot \mathbf{n} = 0 \qquad \text{on } \Gamma, \tag{2.7}$$

where $\mathbf{n}$ denotes the outward unit normal vector of the given surface. Condition (2.6) means that the electric current enters the domain Ω_C perpendicular to the top of the electrodes, whereas condition (2.7) states that the magnetic field is tangential to the boundary. From (2.7) we can assert that there exists a surface potential V, such that $\mathbf{E} \times \mathbf{n} = -\mathrm{grad}V \times \mathbf{n}$ on the surface Γ; moreover, (2.6) implies that V must be constant on each connected component of Γ_C (see, for instance, Bermúdez et al. [18]). To complete the boundary conditions we will fix a ground in the first electrode, where we will impose a null potential ($V = 0$ on Γ_C^1) and on the other two we will prescribe the current, i.e.,

$$\int_{\Gamma_C^n} \mathbf{J} \cdot \mathbf{n} = I_n \quad \text{for } n = 2, 3, \tag{2.8}$$

where I_n are given complex numbers, including the amplitude and phase of the current. Notice that in this model, with 120° phase shift between the electrodes, $I_3 = I_2 e^{\frac{2\pi}{3}i}$. Since current must be preserved, $I_1 = I_2 e^{-\frac{2\pi}{3}i}$.

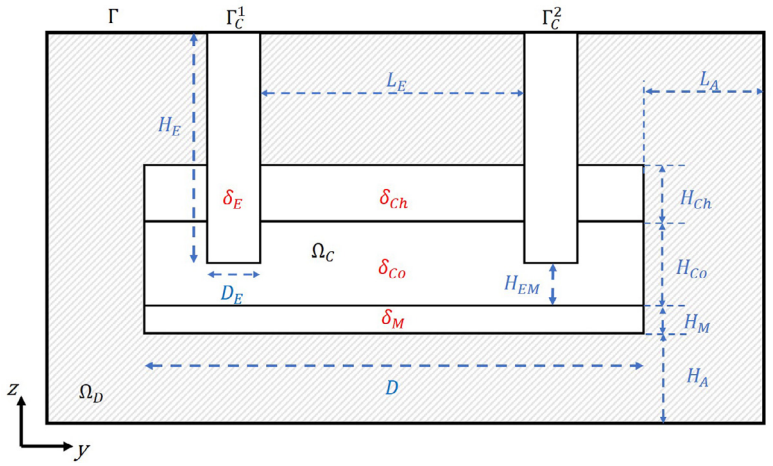

Fig. 2. Sketch of the 2D furnace model with geometric parameters (blue) and skin depths (red). (For interpretation of the references to colour in this figure legend, the reader is referred to the web version of this article.)

Table 1
Geometrical parameters for the reference case.

Parameter	Value [m]	Description
D	10	Furnace diameter
D_E	1.9	Electrode diameter
L_E	4.0	Electrode-electrode distance
H_M	0.5	Metal layer thickness
H_{Co}	2.0	Coke bed layer thickness
H_{Ch}	1.0	Charge layer thickness
H_E	6.3	Total electrode height
H_{EM}	1.7	Electrode-metal distance
H_A	5.0	Distance (z-direction) from conducting parts to the outer boundary
L_A	5.0	Distance (y-direction) from conducting parts to the outer boundary

In what follows, we will introduce numerical tools based on 2D and 1D models obtained from the above equations. First, we will consider a 2D model including only two of the three electrodes of the furnace. This model is intended to provide a *qualitative* analysis rather than a *quantitative* one of how the current is flowing inside the furnace. Next, we will focus on understanding in which situations this 2D model can be reduced to a 1D model in order to develop and exploit analytical solutions for the 1D case.

2.2. 2D model

For the 2D model we will consider a two dimensional domain as the one sketched in Fig. 2 including two electrodes and the same layers of materials as the ones described in the 3D case. The coordinate system has been chosen to coincide with the yz plane of the original xyz system. For this configuration, we assume that the current density is of the form $\mathbf{J} = J_y(y,z)\mathbf{e}_y + J_z(y,z)\mathbf{e}_z$ and there is a phase difference of 180° between the top of the electrodes, instead of 120° as in the previous 3D case. A similar study domain can be found in Karalis et al. [5] for a ferronickel furnace. For simplifying the notation, the domains and boundaries will be denoted in the same way as in the 3D model. We fix a ground in one of the electrodes ($V = 0$ in Γ_C^1). The current is set at the outer boundary Γ_C^2 of the other one assuming it enters perpendicularly.

For solving the 2D model we will use the *Magnetic and Electric Fields* interface of COMSOL Multiphysics v. 5.4 [19], which formulates the problem based on the magnetic vector potential **A** defined by $\mathbf{B} = \mathbf{curl}\ \mathbf{A}$ and the electric scalar potential (V) defined by $\mathbf{E} + i\omega\mathbf{A} = -\text{grad V}$. From the previous assumptions, it can be deduced that **E** and **A** have the same form as **J**, while $\text{V} = \text{V}(y,z)$ and $\mathbf{H} = H_x(y,z)\mathbf{e}_x$. We notice that this software includes the displacement current term of Ampere's law, as it does not increase the computational cost in this harmonic formulation.

We are interested in studying the influence of certain geometrical parameters on the furnace behaviour. More precisely, we have considered 10 independent geometrical parameters determining the domain and which have been detailed in Fig. 2. Typical values for these parameters are specified in Table 1 [10]. In addition, we consider the material properties through the skin depth of each material, which is defined by $\delta = 1/\sqrt{\pi f \mu \sigma}$. Typical values for the average conductivities of the different materials as well as the corresponding skin depth at 50 Hz have been included in Table 2. In what follows, we will refer to the parameter values given in Tables 1 and 2 as the *reference case*.

Table 2
Conductivity (σ) and skin depth (δ) at $f = 50$ Hz; $\mu = \mu_0 = 4\pi \cdot 10^{-7}$ H/m.

Material	σ [S/m]	δ [m]
Charge	0.15	184
Coke bed	500	3.18
Metal	1.5×10^5	0.18
Electrodes	1.5×10^5	0.18

By introducing non-dimensional variables, it is straightforward to show that the governing equation for the electric field in a simple rectangular conductor can be written (in non-dimensional form) as (see, for instance, Schlanbusch et al. [20]):

$$\left(\frac{T}{W}\right)^2 \frac{\partial^2}{\partial \tilde{y}^2}\tilde{\mathbf{E}} + \frac{\partial^2}{\partial \tilde{z}^2}\tilde{\mathbf{E}} - 2i\left(\frac{T}{\delta}\right)^2 \tilde{\mathbf{E}} = \mathbf{0}, \tag{2.9}$$

with δ being the skin depth of the conductor, and W and T being its width and height, respectively. The symbol $\sim$ denotes the non-dimensional variables introduced as $\tilde{x} = Wx$, $\tilde{y} = Ty$ and $\tilde{\mathbf{E}} = E_0\mathbf{E}$, where E_0 is a characteristic value of the electric field. Due to the low frequency operation regime, materials and the system dimensions, the displacement term has been neglected. The qualitative behaviour of the electric field is determined by the two non-dimensional numbers $(T/W)^2$ and $2(T/\delta)^2$. In this case, we have chosen to normalize the equation by the thickness T squared; however, the width W could equally been applied. We may divide the electric behaviour into three different regimes based on the value of $(T/\delta)^2$ [20]:

$$2(T/\delta)^2 \begin{cases} \gg 1 & \text{high skin effect,} \\ \sim 1 & \text{low/moderate skin effect,} \\ \ll 1 & \text{negligible skin effect (DC approximation).} \end{cases} \tag{2.10}$$

We can also argue that there exists three geometric regimes, determined by $(T/W)^2$. For "long and thin" conductors, with $W^2 \gg T^2$, the fields will be approximately 1D. In 1D, the governing equation for the electric field reduces to an analytical solvable ordinary differential equation. The 1D behaviour may occur in both the AC and DC regime.

2.2.1. Selection of parameters to investigate

As announced in previous section, we are interested in studying the influence of the parameters appearing in Fig. 2 on the current and power distribution. If we consider the conductivity and skin depth of each material, we can make some first natural assumptions. In our previous analysis we have shown that we must consider the parameters in terms of the non-dimensional quantities $\left(L_i/L_j\right)^2$ and $2(L_i/\delta_i)^2$, where L_i and L_j are the dimensions of the corresponding subdomain and δ_i includes the material properties. We are mainly interested in what happens within the furnace, so the electrodes themselves are not of interest. Thus, we can neglect the material properties and scales of the electrodes, that is, δ_E and H_E. However, the fact that the electrodes are highly conducting remains important. The air surronding the furnace is added to the model to ensure proper boundary conditions for the magnetic vector potential. The distance from the conducting parts to the outer boundary must be sufficiently large, so that the numerical solution in the interior is not affected. We have evaluated that these parameters are set to reasonable values, so that the numerical solutions are accurate enough. However, the qualitative results will hold even if some numerical precision is lost, and then the parameters H_A and L_A can be ignored in the analysis.

Since the charge layer is low in conductivity and the highly conducting electrodes penetrates the layer, the current will mainly be delivered directly from the electrodes to the coke bed. This means that the current distribution in the electrodes and charge layer does not influence the distribution in the remaining layers significantly. Thus, we can neglect the parameters associated to the charge layer, i.e., δ_{Ch} and H_{Ch}. Further, we assume that the majority of the current flows between the electrodes, thus the electrode distance L_E can be assumed to be more important than the furnace diameter D. When the current leaves the electrodes it may distribute itself, both between the electrodes and down in the metal. Due to the high conductivity of liquid manganese, the skin depth in the metal layer is assumed to be much smaller than the thickness of the layer. As we will show later, the proximity effect between a good conductor and its surroundings may be important. With this is mind, the parameters that define the current distribution in the metal, H_M and δ_M, need to be considered.

In an industrial furnace, the coke bed consists of a mixture of solid coke particles and liquid slag and metal. Hence, the electrical conductivity may vary widely within a small area [15]. However, we consider the layer to be uniform and make a reasonable assumption for the average effective conductivity given in Table 2 which provides a skin depth of the same order as the dimensions of the coke bed. This suggests that variations in the coke bed composition and geometry are important factors for the furnace operation. The current which flows from the electrode tip into the metal will mainly be confined in the area determined by the electrode diameter, D_E, and the electrode-to-metal distance, H_{EM}. Thus, these two parameters are also important. Taking into account the previous considerations, the initial fourteen parameters are reduced to seven, namely D_E, L_E, H_{Co}, H_M, H_{EM}, δ_M and δ_{Co}.

On the other hand, we have stated that we must analyze the non-dimensional numbers $(T/W)^2$ and $2(T/\delta)^2$ instead of the parameters themselves. Numerical values for selected ratios are given in Table 3 for the reference case. Notice that

Table 3
Non-dimensional numbers for the reference case scenario, with parameters given in Table 1.

	Width W	Height T	$(T/W)^2$	$2(T/\delta)^2$
Electrodes	H_E	D_E	0.09	223
Charge	L_E	H_{Ch}	0.06	6E5
Coke bed*	L_E	H_{Co}	0.25	0.79
Electrode-Metal**	H_{EM}	D_E	1.25	0.71
Metal	L_E	H_M	0.015	15

* Between electrodes.
** Coke bed below electrode tip.

the non-dimensional numbers corresponding to electrodes are only included to illustrate the skin effect and 1D behaviour within them.

We note that the assumption "long and thin" is reasonable for the electrode, the charge and the metal. However, the numerical values suggest that the coke bed layer should be handled with care. For both the electrodes and the metal layer, we are clearly in the high skin effect regime, and we have a 1D behaviour in the centre of each material. In the coke bed, we have that the current distribution is in the low skin effect regime.

2.3. 1D model

In "long and thin" conductors, the model for the electric field can be further reduced. More precisely, there will only be electric current in the length direction, and **E** is adequately described by the unidimensional equation:

$$\frac{d^2}{dz^2}E_y(z) - \frac{2i}{\delta^2}E_y(z) = 0. \tag{2.11}$$

This equation can be solved analytically by providing suitable boundary conditions. In [21] a general solution is derived for the full Maxwell system by considering the electromagnetic wave equation. In this work we consider a similar 1D model derived from the low-frequency estimate of the wave equation. The model can be solved for any number of material layers, which would represent the different layers in a smelting furnace.

As a comparable 1D model for the 2D furnace model stated in Section 2.2, we consider a three layer domain, including the coke bed, metal, and air (dielectric) below the furnace. We ignore the charge layer since, due its low conductivity, we can assume $J_y = 0$. The air layer extends to infinity, and thus only a boundary condition is needed at the top domain. Let E_j, $j = 1, 2, 3$ denote the electric field distribution in the coke bed, metal and dielectric layer, respectively. The general solution to Eq. (2.11) is then given by

$$E_j(z) = A_j e^{-\alpha z/\delta_j} + B_j e^{\alpha z/\delta_j} \qquad \text{for } j = 1, 2, \tag{2.12}$$

$$E_3(z) = A_3 z + B_3, \tag{2.13}$$

where $\alpha = 1 + i$. The unknown coefficients A_j and B_j, $j = 1, 2, 3$ can be determined from the following boundary conditions

$$E(z) = E_0 \qquad \text{at } z = 0, \tag{2.14}$$

$$E_j(z) = E_{j+1}(z) \qquad \text{at } z = Z_j,\ j = 1, 2, \tag{2.15}$$

$$\frac{1}{\mu_j}\frac{d}{dz}E_j(z) = \frac{1}{\mu_{j+1}}\frac{d}{dz}E_{j+1}(z) \qquad \text{at } z = Z_j,\ j = 1, 2, \tag{2.16}$$

$$|E(z)| < C \qquad \forall z, C \text{ being a positive constant}, \tag{2.17}$$

where Z_j, $j = 1, 2$ denote the position of the interface between layers j and $j + 1$. We obtain the following expressions in terms of E_0:

$$A_1 = \frac{E_0}{1 + \frac{(\gamma_1/\gamma_2)-1}{(\gamma_1/\gamma_2)+1}e^{-2\alpha Z_1/\delta_1}}, \tag{2.18}$$

$$B_1 = E_0 - A_1, \tag{2.19}$$

$$A_2 = \frac{1}{\gamma_1}\left(A_1 e^{-\alpha Z_1/\delta_1} + B_1 e^{\alpha Z_1/\delta_1}\right), \tag{2.20}$$

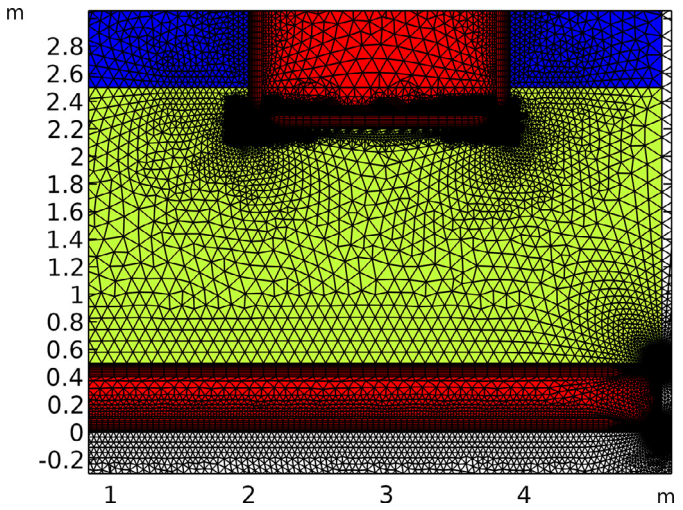

Fig. 3. Mesh for the reference case in the region surrounding the right electrode. The colours indicate the different materials.

$$B_2 = A_2 e^{-2\alpha Z_2/\delta_2}, \tag{2.21}$$

$$A_3 = 0, \tag{2.22}$$

$$B_3 = A_2 e^{-\alpha Z_2/\delta_2} + B_2 e^{\alpha Z_2/\delta_2}, \tag{2.23}$$

where we have introduced

$$\gamma_1 = e^{-\alpha Z_1/\delta_2} + e^{\alpha(Z_1-2Z_2)/\delta_2}, \tag{2.24}$$

$$\gamma_2 = \frac{\mu_1}{\mu_2}\frac{\delta_1}{\delta_2}\left(e^{-\alpha Z_1/\delta_2} - e^{\alpha(Z_1-2Z_2)/\delta_2}\right). \tag{2.25}$$

3. Numerical case studies

We have solved the 2D model with COMSOL Multiphysics v. 5.4 using the *Magnetic and Electric Fields* interface. We recall the reference case corresponds to the geometric parameters and material properties given in Tables 1 and 2, respectively. We are interested in analysing the sensitivity of the electric current and power distribution with respect to different parameters. To ensure a well-defined mesh for each different parameter setting, the size of the elements is related to the skin depth in the most conductive materials, i.e., in electrodes and metal. In particular, on the surface of these materials we defined a boundary layer composed of rectangular elements, which allows us to increase the resolution in the direction normal to the surface without greatly increasing the overall mesh size. We have also refined the mesh in the region surrounding the electrode tips and at the corners. A detail of the mesh constructed from these guidelines for the reference case is shown in Fig. 3. The different materials are indicated by the background color.

3.1. Numerical simulations of 2D model

The current density and power density distributions for the reference case are shown in Fig. 4. The skin effect is relevant in both electrodes and metal. Moreover, due to the proximity effect of the two electrodes, the current concentrates near the inward walls. The current distributes more uniformly in the coke bed layer. Some of the current flows directly between the electrodes in the upper part, while some flows down into the metal. Further, we note that there is only a negligible amount of current flowing in the charge layer.

The power density shows that the majority of power is being generated in the coke bed region. However, we note that there is some concentration of power generation in the surface layers of the metal and electrodes. The figures show a good agreement with the interpretation of the non-dimensional numbers in Table 3.

In Table 4 we have calculated the total (2D) power [MW/m] generated in each part of the furnace. The electrode power is included as it is descriptive for the model. However, since the electrode length is somewhat arbitrarily chosen, the value itself is not important.

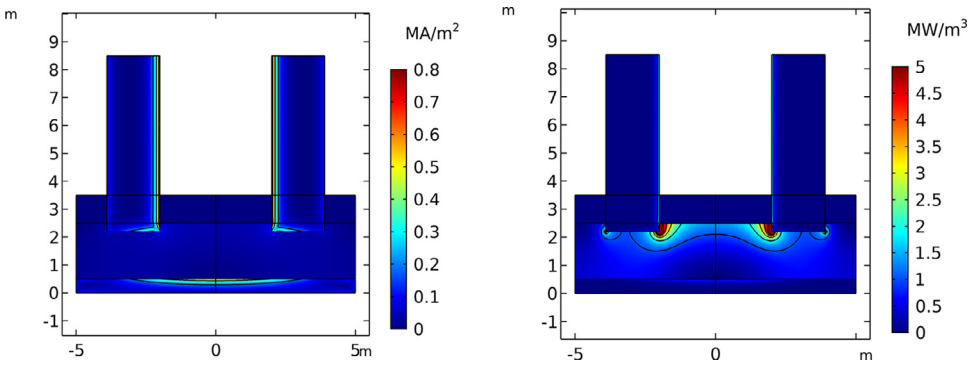

Fig. 4. Current density (left) and power density (right) distribution in the 2D furnace model for the reference case.

Table 4
Power in the different regions for the reference case with input current $I_0 = 115$ kA.

Region	P [MW/m]	P[%] of total
Electrodes	2.3	13
Charge	0.004	0.02
Coke bed	14.9	84.5
Metal	0.44	2.5
Total	17.6	100

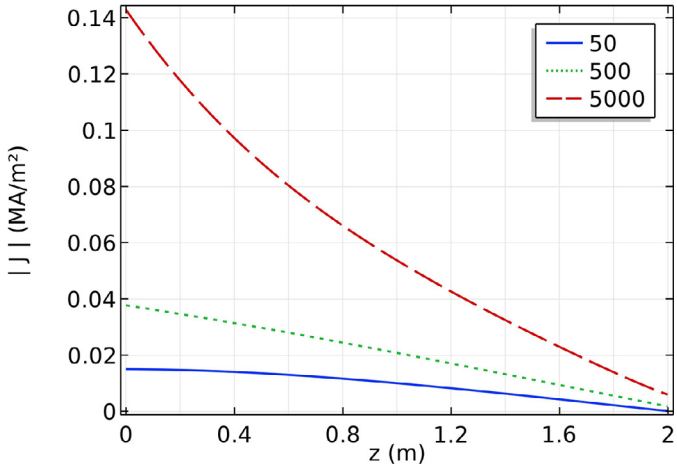

Fig. 5. Current density norm in the coke bed center ($y = 0$) for different values of coke bed conductivity. The middle curve represents the reference case with $\delta_{Co} = 500$ S/m, $z = 0$ corresponds to the coke bed top.

We are interested in how the behaviour of the electrical distribution changes with the parameters. The values in Table 3 suggest that the distribution is most sensitive to changes in the coke bed, as the non-dimensional numbers are of $\mathcal{O}(1)$. In particular, we want to know how the current flows through the coke bed. One way to describe the distribution is to consider the horizontal currents through the furnace center. This shows how deep the current flows in the furnace, and to what extent it flows through the metal. In Fig. 5 we show the current density across the vertical cross section at the coke bed centre. The three curves represent different values for the coke bed conductivity, the dotted line being the reference case value. The input current is kept constant (at 115 kA) for each case. We see that the changes in the coke bed conductivity change both the total amount of horizontal current passing through it and the internal distribution of the current. There is an accumulation of horizontal currents in the top of the coke bed for all three cases. This indicates that a DC model will not give an accurate description of horizontal currents, even at low/moderate coke bed conductivity as the accumulation of current is caused by induction.

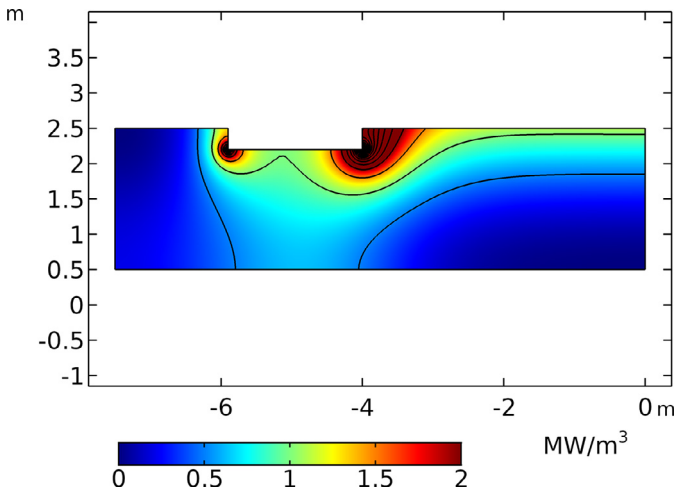

Fig. 6. Power density in the left side of coke bed of a *long and thin* furnace. The contour lines indicate levels of constant power with a difference of 0.5 MW/m^3.

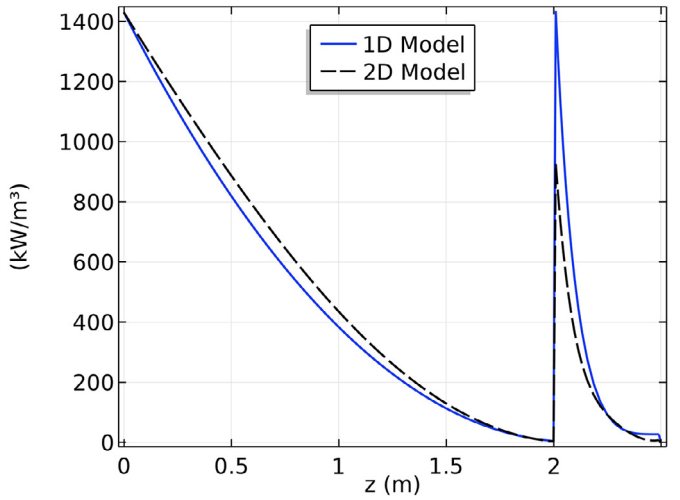

Fig. 7. Power density at furnace center for the reference case. The range is from the coke bed top ($z = 0$) to the metal bottom ($z = 2.5$).

3.2. Validation and application of 1D model

Our analysis has shown that a 1D model of the electric field is valid for long and thin conductors. In order to validate the analysis we have first performed simulations with an unrealistic long furnace model. The distance between the electrodes is set to 8 m and the total furnace width is extended accordingly. The remaining parameters are kept equal to the reference case model, which gives us $(H_{Co}/L_E)^2 = 0.0625 \ll 1$, which is clearly in the *long and thin* regime. In Fig. 6 we plot the power distribution on the left side of the coke bed. The included contour lines show that the electric behaviour is 1D outside of a boundary region around the electrode tip. Thus, the numerical simulation agrees with the analysis.

Since the 2D furnace model is symmetric, the current is forced to be horizontal in the furnace centre, and thus, the fields will be 1D. In Fig. 7 we plot the power density along the vertical cross section at the furnace center. We compare the results calculated by the analytical 1D model and numerical 2D model for the reference case scenario. The 1D model relies on input from the 2D model, in terms of the calculated (measured) field value at $z = 0$. We consider only the results for the coke bed and metal layer, and neglect the low conducting charge. We see that the two models agree quite well in the coke bed, while the deviation is larger in the top surface of the metal. We have made this comparison for different cases, by calculating the deviation, which we define as

$$\kappa = \frac{\int |P_{1D}(z) - P_{2D}(z)| dz}{\int P_{2D}(z) dz}, \tag{3.1}$$

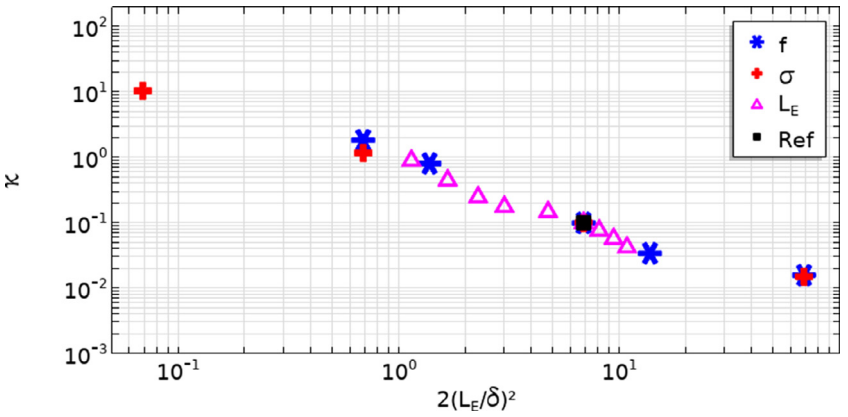

Fig. 8. Log-log plot of the deviation of 1D estimate for different parameter settings. $2(L_E/\delta)^2$ is changed by either changing f, σ or L_E, while keeping the other two parameters constant. The reference case is indicated by a black dot.

Table 5
Total power [MW/m] generated in coke bed, calculated by DC and AC model for different electrode positions.

	H_{EM} [m]			
	1.7	1.2	0.7	0.2
DC	11.7	8.4	5.4	2.1
AC	14.9	11.4	8.6	5.8
Difference	3.2	3.0	3.2	3.7

where the line integrals are evaluated from the coke bed top to the middle of the metal layer. The values of the power P_{1D} and P_{2D} are obtained from the formula $P = |\mathbf{J}|^2/2\sigma$ applied to the 1D and 2D model, respectively. In the 1D model, we only have a horizontal field so that $\mathbf{J} = J_y\mathbf{e}_y$. Due to the symmetry of the 2D model, the current density vector takes the same form as in the 1D model, as the vertical component must be zero. The 1D model is unable to describe the horizontal currents in the outer skin of the metal, as they are to a large extent caused by 2D effects. Therefore, in order to neglect a systematic error we disregard the bottom half of the metal. By this numerical inspection we have found that the 1D estimate is most sensitive to variations in the relationship between the electrode distance and the coke bed skin depth. In Fig. 8 we show the deviations for three different studies. We consider changes in the non-dimensional number $2(L_E/\delta)^2$ by either changing the frequency f, the coke bed conductivity σ or the electrode distance L_e, while keeping the other two parameters constant. Notice that for the reference case, indicated in the figure by a black dot, we have a deviation of about 10%. We notice from the results that the deviation decreases when the electrode distance increases or the coke bed skin depth decreases. In other words, the numerical results agree with the analysis.

3.3. AC models vs. DC models

We have implemented a 2D DC model to be compared with the AC simulations. For the DC model we only allow the current to flow in a surface layer of thickness δ in the electrodes and metal, in order to mimic the skin effect. Due to the strong proximity effect as seen in Fig. 4, only the inward part of the electrodes are included. In Table 5 we have given the total generated power obtained by the AC and DC models for different electrode positions. There is a significant difference between DC and AC for all cases. The absolute difference is approximately constant for all of the electrode positions. This means that the horizontal currents are independent of the electrode depth.

The vality of DC models may also be estimated by applying the analytical 1D model. Consider a two-layered 1D model, representing the coke bed and the metal layer of the 2D furnace. We consider both an AC model as described in Section 2.3 as well as a simple 1D DC model. Similarly to the 2D DC model, we restrict the metal layer to a thickness δ. In the AC model we consider the metal layer to be infinite, which is reasonable when the skin depth is small compared to the thickness. The current is kept constant equal to the reference case ($I_{AC} = 115$ kA) and $I_{DC} = I_{AC}/\sqrt{2}$. In Fig. 9 we plot the (1D) power densities, defined as $p_{AC}(z) = \sigma(z)|E(z)|^2/2$ and $p_{DC}(z) = \sigma(z)|E(z)|^2$ for the AC and DC model, respectively. We see that the difference between AC and DC increases as the coke bed conductivity increases. Moreover, we see that the 1D model estimates a significant difference between AC and DC even at moderate conductivities, in accordance with the current densities shown in Fig. 5.

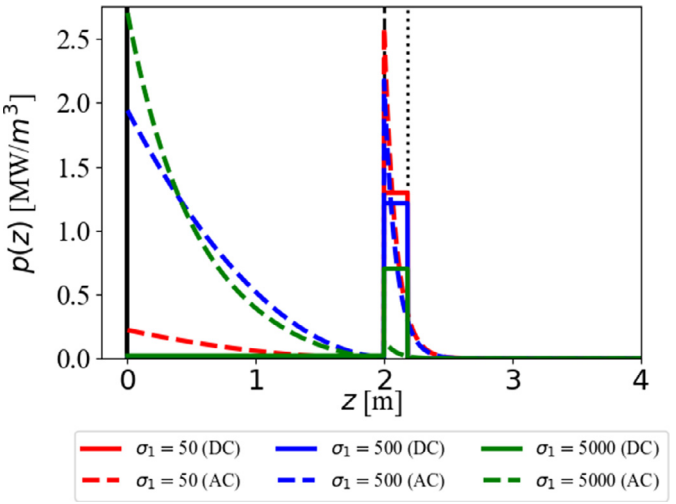

Fig. 9. 1D Power densities by AC (dotted lines) and DC (solid lines) with coke bed conductivity equal to 50 S/m (red), 500 S/m (blue) and 5000 S/m (green). The layer interface is at $z = 2$ m, while the skin depth of the metal is indicated by a dotted vertical line at $z = 2.18$ m. (For interpretation of the references to colour in this figure legend, the reader is referred to the web version of this article.)

4. Conclusions

Our analysis and case studies show that 2D and 1D models are valuable tools to acquire insight into qualitative aspects for current paths in large metallurgical furnaces. The electrical current distribution within the furnace is governed by two types of non-dimensional numbers, $(T/W)^2$ and $2(T/\delta)^2$, i.e., squared geometric aspect ratios and squared ratio between a length/thickness and the respective skin depth.

With reasonable (typical) material properties and dimensions, the electrical distribution in the furnace is most sensitive to changes in coke bed shape and composition. The highly conductive electrodes and metal layer will largely affect the current distribution in the less conductive neighbouring materials. This will reinforce the AC effects in the furnace as a whole, and “push” parallel currents in the coke bed away from the metal and electrodes.

If the power due to parallel currents in the coke beds is significant, AC computations will differ substantially from DC. If, however, the furnace power is dominated by vertical currents, DC simulations can be relevant.

Our 1D and 2D studies do not claim to replace 3D simulations, which will be needed for determining in more detail the behaviour in the furnace. However, they can be additional and simpler tools to understand inductive effects and the sensitivity with respect to different physical and geometrical parameters.

Acknowledgements

This paper is published as part of the project Electrical Conditions and their Process Interactions in High Temperature Metallurgical Reactors (ElMet) 247791, with Financial support from The Research Council of Norway and the companies Elkem and Eramet Norway.

References

[1] S.A. Halvorsen, H.A.H. Olsen, M. Fromreide, An efficient simulation method for current and power distribution in 3-phase electrical smelting furnaces, IFAC-PapersOnLine 49 (20) (2016) 167–172.
[2] Y.Y. Sheng, G.A. Irons, D.G. Tisdale, Transport phenomena in electric smelting of nickel matte: part II, mathematical modeling, Metall. Mater. Trans. B 29.1 (1998) 85–94.
[3] M. Dhainaut, Simulation of the electric field in a submerged arc furnace, in: Proceedings of the Tenth International Ferroalloy Congress, 2004, pp. 605–613.
[4] D. Darmana, J.E. Olsen, K. Tang, E. Ringdalen, Modelling concept for submerged AC furnaces, in: Proceedings of the Ninth International Conference on CFD in the Minerals and Process Industries, Melbourne, Australia, 2012.
[5] K.T. Karalis, N. Karkalos, N. Cheimarios, G.S.E. Antipas, A. Xenidis, A.G. Boudouvis, A CFD analysis of slag properties, electrode shape and immersion depth effects on electric submerged arc furnace heating in ferronickel processing, Appl. Math. Model. 40 (21-22) (2016) 9052–9066.
[6] K. Karalis, N. Karkalos, G.S.E. Antipas, A. Xenidis, Pragmatic analysis of the electric submerged arc furnace continuum, R. Soc. Open Sci. 4 (2017), doi:10.1098/rsos.170313.
[7] K. Karalis, N. Karkalos, G.S.E. Antipas, A. Xenidis, Computational fluid dynamics analysis of a three-dimensional electric submerged arc furnace operation, 10.31219/osf.io/xgnse, last access 1.dec.2020.
[8] Y.A. Tesfahunegn, T. Magnusson, M. Tangstad, G. Saevarsdottir, Effect of electrode shape on the current distribution in submerged arc furnaces for silicon production - a modelling approach, J. South Afr. Inst. Min. Metall. 118 (2018) 595–600, doi:10.17159/2411-9717/2018/v118n6a6.
[9] I. McDougall, Finite element modelling of electric currents in AC submerged arc furnaces, Infacon XI: International Ferro-Alloys Congress, New Delhi, India, 2007.

[10] E.V. Herland, M. Sparta, S.A. Halvorsen, 3D-models of proximity effects in large FeSi and FeMn furnaces, J. South Afr. Inst. Min. Metall. 118 (2018) 607–618.
[11] E.V. Herland, M. Sparta, S.A. Halvorsen, Skin and proximity effects in electrodes and furnace shells, Metall. Mater. Trans. B 50 (2019) 2884–2897, doi:10.1007/s11663-019-01651-8.
[12] Y.A. Tesfahunegn, T. Magnusson, M. Tangstad, G. Saevarsdottir, Dynamic current and power distributions in a submerged arc furnace, in: G. Lambotte, J. Lee, A. Allanore, S. Wagstaff (Eds.), Materials Processing Fundamentals 2019, The Minerals, Metals & Materials Series, Springer, 2019.
[13] Y.A. Tesfahunegn, T. Magnusson, M. Tangstad, G. Saevarsdottir, Comparative study of AC and DC solvers based on current and power distributions in a submerged arc furnace, Metall. Mater. Trans. B 51 (2020) 510–518, doi:10.1007/s11663-020-01794-z.
[14] S.E. Olsen, M. Tangstad, T. Lindstad, Production of Manganese Ferroalloys, Tapir Academic Press, 2007.
[15] P.A. Eidem, Electrical Resistivity of Coke Beds, Norwegian University of Science and Technology, 2008 Ph.D. thesis.
[16] S.O. Wasbø, Ferromangenese Furnace Modelling Using Object-Oriented Principles, Norwegian University of Science and Technology, 1996 Ph.D.thesis.
[17] A. Bossavit, Computational Electromagnetism, Academic Press Inc, San Diego, CA, 1998.
[18] A. Bermúdez, D. Gómez, P. Salgado, Mathematical Models and Numerical Simulation in Electromagnetism, Springer International Publishing, 2014.
[19] C. Multiphysics, AC/DC module user's guide, v 5.4, 2018.
[20] R. Schlanbusch, S.A. Halvorsen, S. Shinkevich, D. Gómez, Electrical Scale-up of Metallurgical Processes, COMSOL Conference, Cambridge, UK, 2014.
[21] H.W. Deng, Y.J. Zhao, C.J. Liang, W.S. Jiang, Y.M. Jing, Effective skin depth for multilayer coated conductor, Prog. Electromagn. Res. M 9 (2009) 1–8.